ФЕДЕРАЛЬНОЕ ГОСУДАРСТВЕННОЕ АВТОНОМНОЕ ОБРАЗОВАТЕЛЬНОЕ
УЧРЕЖДЕНИЕ ВЫСШЕГО ОБРАЗОВАНИЯ
«НАЦИОНАЛЬНЫЙ ИССЛЕДОВАТЕЛЬСКИЙ УНИВЕРСИТЕТ
«ВЫСШАЯ ШКОЛА ЭКОНОМИКИ»

МОСКОВСКИЙ ИНСТИТУТ ЭЛЕКТРОНИКИ И МАТЕМАТИКИ
им. А.Н. ТИХОНОВА

Ефремов Виктор Васильевич, группа БИТ203

ЧИСЛЕННОЕ МОДЕЛИРОВАНИЕ ВОЛЬТ-АМПЕРНЫХ ХАРАКТЕРИСТИК МЕЗОСКОПИЧЕСКИХ СВЕРХПРОВОДНИКОВ

Выпускная квалификационная работа
по направлению 11.03.02 Инфокоммуникационные технологии и системы связи
студента образовательной программы бакалавриата
«Инфокоммуникационные технологии и системы связи»

Студент

В.В. Ефремов
И.О. Фамилия

Руководитель
ученая степень, звание (при наличии)

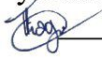

д. Т.Тейшейра Сарайва
И.О. Фамилия

Москва 2024 г.

ФЕДЕРАЛЬНОЕ ГОСУДАРСТВЕННОЕ АВТОНОМНОЕ ОБРАЗОВАТЕЛЬНОЕ УЧРЕЖДЕНИЕ ВЫСШЕГО ОБРАЗОВАНИЯ
«НАЦИОНАЛЬНЫЙ ИССЛЕДОВАТЕЛЬСКИЙ УНИВЕРСИТЕТ
«ВЫСШАЯ ШКОЛА ЭКОНОМИКИ»

МОСКОВСКИЙ ИНСТИТУТ ЭЛЕКТРОНИКИ И МАТЕМАТИКИ
им. А.Н. ТИХОНОВА

ЗАДАНИЕ
на выпускную квалификационную работу бакалавра

студенту группы БИТ-203 Ефремову Виктору Васильевичу

1. Тема работы

Numerical Simulation of Voltage-Ampere Characteristics of Mesoscopic Superconductors

2. Требования к работе

During the work, the following stages must be completed: Obtain the discrete form of the TDGL equations in non-orthogonal coordinates in the link variables formulation (gauge invariant form). Write a computational code to perform simulations of a superconducting thin film submitted to an external magnetic field and/or applied current. Construct a phase diagram of the vortex dynamics.

3. Содержание работы

Contents of the work: abstract, introduction, theoretical methods, results and discussion, conclusion, and bibliography.

4. Сроки выполнения этапов работы

Проект ВКР представляется студентом в срок до	«20» декабря 2023 г.
Первый вариант ВКР представляется студентом в срок до	«20» апреля 2024 г.
Итоговый вариант ВКР представляется студентом руководителю до загрузки работы в систему «Антиплагиат» в срок до	«10» мая 2024 г.

Задание выдано «20» декабря 2023 г. _____ Т. Тейшейра Сарайва
подпись руководителя

Задание принято к исполнению «20» декабря 2023 г. _____ В.В. Ефремов
подпись студента

Abstract

The time dependent Ginzburg-Landau equations (TDGL) describe the dynamic of superconductors. In this work, we generalize a numerical method for integrating the TDGL equations. We formulated them in skew coordinates and also developed a discrete form to study dynamics of Abrikosov vortices generated by applied magnetic field, current. We verified the angle dependence of the response of the system with respect to these parameters. We study superconducting properties of a parallelogram-shaped thin film surrounded by ferromagnetic material and immersed in an external magnetic field applied perpendicular to its plane with and without presence of current. The Link variables method is used in conjunction with skew coordinates and method of fractional steps. The results of the thesis are important for understanding the behaviour of superconducting nanodevices that range from studies in fundamental physics to commercial ultra-fast detectors.

The work consists of 28 pages, contains 8 figures and 18 references.

Аннотация

Зависящие от времени уравнения Гинзбурга-Ландау описывают поведение сверхпроводников. В этой работе мы обобщаем численный метод решения уравнений Гинзбурга-Ландау. Мы формулируем их в косоугольных координатах в непрерывной и дискретной формах чтобы изучить вихри Абрикосова возникающие при приложении магнотного поля, тока. Мы подтвердили зависимость отклика системы от угла. В работе исследованы свойства тонких свехпроводящих пленок окруженных ферромагнетиком в перпендикулярном магнитном поле, в присутствии тока и без. Метод связанных переменных используется вместе с косоугольными координатами и методом дробных шагов. Результаты этой работы важны для понимания поведения серхпроводниковых устройств от фундаментальных исследований до сверхскоростных детекторов.

Работа сдержит 28 страниц, 8 рисунков и 18 литературных источников.

Contents

1 Terminology

There are several very widespread superconductivity-related terms and names. We list them here for the convenience's sake.

Penetration depth (length) λ is the depth at which intensity of magnetic field damps to $1/e$ of its value on the boundary.

Coherence length ξ is characteristic distance of order parameter variance. On length scale much smaller than ξ order parameter Ψ changes negligibly.

Order parameter Ψ is complex-valued function that is used in Ginzburg-Landau theory. If $\Psi = 0$ the material is normal, non-superconducting. If Ψ is not zero the material is superconducting.

Ginzburg-Landau parameter $\kappa = \lambda/\xi$ is a ratio of two characteristic lengths. It determines if superconductor of *type-I* ($\kappa < 1/\sqrt{2}$) or *type-II* ($\kappa > 1/\sqrt{2}$). Two types of superconductor behaves very differently in response to applied magnetic field.

2 Introduction

Superconductivity is characterized by zero electrical resistance and screening of magnetic field. Former means that electrical current do not dissipate and can persist infinitely. Latter, which is also called Meissner effect, means that magnetic field do not penetrate the body of superconductor. To be more precise — external magnetic field rapidly exponentially damps with depth typically losing several orders of magnitude at micrometres depth.

Initially superconductivity was experimentally discovered in 1911 by Dutch physicist Heike Kamerlingh Onnes as described in [1]. Few years prior he liquefied helium which boils at 4.2K. That gave a rise to all sorts of low-temperature experiments including the one that lead to discovery of superconductivity.

Superconductivity is quantum phenomenon — to properly explain behaviour of superconductor one have to resort to quantum mechanics. There are theories that do exactly this, for example widely used Bardeen–Cooper–Schrieffer (BCS) theory introduced in 1957 in [2]. Nevertheless we use Ginzburg-Landau (GL) theory in this study. On the one hand GL equations are relatively simple, on the other it provides precision that good enough for many applications.

Practical applications of superconductivity are somewhat limited because even high-temperature superconductors operate at temperature well under hundred degree Celsius below zero. Still, there are many examples of successful applications of superconducting devices at the edge of science and technology. Having no electrical resistance superconductors make an excellent choice for extremely powerful electromagnets, which used in magnetic resonance imaging (MRI) – a widespread diagnosis tool in modern medicine. Maglev (from magnetic levitation) is another device that uses superconducting magnets. It is a type of train that floats over rail. Lack of physical contact eliminates friction drastically raising maximum speed with current record being 600 km/h. There are also quantum computers. Qubits which quantum computer is made of can be physically implemented as superconducting circuits. Another very promising area of research is quantum cryptography and quantum communication. In theory those methods of cryptography is absolutely secure because of laws of physics. Even though the technology still in development phase it created demand for niche tools, such as *single photon detectors* – devices that can count separate photons, distinguishing one photon from two. Lastly, there are SQUIDs (superconducting quantum interference device). It is extremely sensitive magnetometer that is built on Josephson

junctions.

Thanks to development of superconducting industry there is an increasing demand in computer simulation tools and frameworks that are used to design devices and test new ideas. It is the primal reason of relevance of our study. We hope to introduce new technique that will improve existing computational methods.

There are multiple papers on GL in non-cartesian coordinates or specific shapes. Dai and Lappicy discussed GL in spherically symmetric case in [3]. Barba Ortega *et al*. did it for disc in [4]. We follow same path and study GL in skew coordinates.

In the study we focus on numerical solution of GL equations. We rewrite the equations in skew coordinates and apply link-variables method. After discretization we apply method of fractional steps and obtain numerical solution for various shapes. Finally we visualize data and discuss results.

3 Ginzburg-Landau theory

In 1937 in [5] Lev Landau presented theory of continuous phase transitions, which later lead to new approach to theoretical explanation of superconductivity. In 1950 in collaboration with Vitaly Ginzburg he published [6].

The key part of the theory is *order parameter* Ψ, a complex-valued function that describes state of matter. Material is normal, non-superconducting when $\Psi = 0$. And superconducting if Ψ is not zero. Surprisingly, such a simple assumption led to quite powerful theory.

Expansion of free energy in terms of powers of Ψ and minimization of following expression leads to GL equations, a pair of differential equations involving order parameter and vector potential.

3.1 Gauge invariance

Electromagnetic field can be described in terms of *potentials* — a vector potential $\vec{A}$ and a scalar potential φ

$$\vec{B} = \nabla \times \vec{A} \tag{1}$$

$$\vec{E} = -\nabla\varphi - \frac{\partial \vec{A}}{\partial t} \tag{2}$$

Important point is the potentials are not unique. If we apply a gauge transformation

$$\vec{A} \to \vec{A} + \nabla\psi \tag{3}$$

$$\varphi \to \varphi - \frac{\partial \psi}{\partial t} \tag{4}$$

where ψ is arbitrary smooth enough function of coordinate and time, the electromagnetic field remains the same. Therefore there is some freedom in selection of potential.

In this work we use *Weyl gauge*

$$\varphi = 0 \tag{5}$$

because it simplifies GL equations quite significantly.

3.2 TDGL equations

Using auxiliary operator $\vec{D} = \vec{\nabla} - i\frac{2e}{\hbar c}\vec{A}$ we can write time-dependent GL equations in the following form

$$-\frac{\mathcal{K}}{D}\left(\partial_t + i\frac{2e}{\hbar}\varphi\right)\Psi = a(1 - T/T_c)\Psi + b|\Psi|^2\Psi - \mathcal{K}\vec{D}^2\Psi \tag{6}$$

$$\frac{\sigma}{c}\left(\vec{\nabla}\varphi + \frac{1}{c}\partial_t\vec{A}\right) = i\mathcal{K}\frac{2e}{\hbar c}\left(\Psi\vec{D}^*\Psi^* - \Psi^*\vec{D}\Psi\right) - \frac{1}{4\pi}\vec{\nabla}\times\vec{\nabla}\times\vec{A} \tag{7}$$

Where Ψ is an order parameter, a, b and $\mathcal{K}$ are GL coefficients, $\vec{A}$ is vector potential, ϕ is scalar potential, σ is conductivity, D is the diffusion constant, T is the temperature, T_C is the critical temperature, e is the electron charge, c is the speed of light, $\hbar$ is the reduced Planck constant.

Coupled with boundary conditions those equations can be used for simulation of real world superconductors.

3.3 Dimensionless units

It is beneficial to use *dimensionless units*, i.e. express everything as ratios to base units:

$$\text{Order Parameter} \quad \Psi_0 = \sqrt{\frac{|a|(1-T/T_c)}{b}}$$

$$\text{Distances} \quad \xi(T) = \sqrt{\frac{\mathcal{K}}{|a|(1-T/T_c)}}$$

$$\text{Time} \quad t_0 = \frac{\xi^2}{D}$$

$$\text{Vector Potential} \quad A_0 = \frac{\Phi_0}{2\pi\xi}$$

$$\text{Scalar potential} \quad A_0$$

$$\text{Current} \quad \frac{A_0}{c\sigma_n t_0}$$

where $\Phi_0 = hc/2e$ is quantum of magnetic flux. Finally the equations look like

$$\partial_t\Psi = \vec{D}^2\Psi + (1 - |\Psi|^2)\Psi \tag{8}$$

$$\sigma'\partial_t\vec{A} = i\left(\Psi\vec{D}^*\Psi^* - \Psi^*\vec{D}\Psi\right) - \kappa^2\vec{\nabla}\times\vec{\nabla}\times\vec{A}, \tag{9}$$

where $\sigma' = \frac{\sigma D}{c^2}$ is the renormalized conductivity, which gives the ratio between characteristic time of variations between the order parameter and vector potential. Important note, in dimensionless units $\vec{D} = \vec{\nabla} - i\vec{A}$.

3.4 Thin film limit

In the work we consider thin film superconductor. We choose to align external magnetic field in such a way that it will be perpendicular to plane of the film. We also fix coordinate system so the film lays in xOy coordinate plane and magnetic field has only z-component B_z.

It leads to few more simplifications. First, in thin films Ginzburg-Landau parameter κ depends on the thickness of the film d

$$\kappa = \frac{\lambda^2}{d\xi} \tag{10}$$

making it effectively infinite for small d [7]. Therefore $\vec{\nabla} \times \vec{\nabla} \times \vec{A}$ must be zero. Combined with the fact that magnetic field has only z-component leads to the fact $B_z = const$ — the magnetic field is spatially constant. Because of it we can discard the **??** for vector potential.

Second, because the film is very thin, the magnetization is negligible and we can assume that external magnetic field $\vec{H}_e$ and local magnetic field $\vec{B}$ are equal.

With thin film limit assumptions general time-dependent Ginzburg-Landau equations simplifies to

$$\partial_t \Psi = \kappa \vec{D}^2 \Psi + \left(1 - |\Psi|^2\right) \Psi \tag{11}$$

where once again, $\vec{D} = \vec{\nabla} - i\vec{A}$. This is the equation we will study.

4 Skew coordinates

Skew coordinates is a curvilinear coordinate system which axes are not orthogonal, i.e. an angle between basis vectors is not right. Skew coordinates are harder to work with compared to cartesian coordinates because the metric tensor has non-zero off-diagonal elements, which leads, for example, to more complicated formulas in vector calculus. Still, in some cases skew coordinates are beneficial. For instance, differential equations in parallelogram areas.

In this section we use prime to denote objects (vectors, coordinates, derivatives, *etc.*) related to skew coordinate system. And non-primed version for their cartesian coordinates counterparts.

Let $\mathbf{i}$, $\mathbf{j}$ be unit basis vectors in 2D cartesian coordinates. Let us define new basis vectors:

$$\mathbf{i}' = \mathbf{i} \tag{12}$$

$$\mathbf{j}' = \sin\phi\mathbf{i} + \cos\phi\mathbf{j} \tag{13}$$

Where ϕ is a complementary to the angle between axes. So, for example, cartesian coordinates can be considered skew coordinates with $\phi = 0$.

We can also define old (cartesian, non-primed) basis in terms of new (skew, primed):

$$\mathbf{i} = \mathbf{i}' \tag{14}$$

$$\mathbf{j} = -\tan\phi\mathbf{i}' + \sec\phi\mathbf{j}' \tag{15}$$

Relation between cartesian coordinates and skew coordinates goes as follows

$$x' = x - \tan\phi y \tag{16}$$

$$y' = \sec\phi y \tag{17}$$

And other way around

$$x = x' + \sin\phi y' \tag{18}$$
$$y = \cos\phi y' \tag{19}$$

Each vector can be represented by its *coordinates* — a pair of numbers, which depends on chosen coordinate system. For example, consider arbitrary vector $\vec{V}$

$$\vec{V} = V_x\mathbf{i} + V_y\mathbf{j} = V'_x\mathbf{j}' + V'_y\mathbf{j}' \tag{20}$$

Then its x-coordinate can be written in terms of x' and y' coordinates

$$V_x = V'_x + \sin\phi V'_y \tag{21}$$

Relation between derivatives can be obtained using chain rule

$$\partial_x = \partial_{x'}\frac{\partial x'}{\partial x} + \partial_{y'}\frac{\partial y'}{\partial x} = \partial_{x'} \tag{22}$$
$$\partial_y = \partial_{x'}\frac{\partial x'}{\partial y} + \partial_{y'}\frac{\partial y'}{\partial y} = -\tan\phi\partial_{x'} + \sec\phi\partial_{y'} \tag{23}$$

Similarly it is possible to show that divergence of a vector field is a sum of partial derivatives

$$\vec{\nabla}\cdot\vec{V} = \partial_{x'}V'_x + \partial_{y'}V'_y \tag{24}$$

And Laplacian of a scalar field

$$\Delta\Psi = \sec^2\phi\ \partial^2_{x'}\Psi + \sec^2\phi\partial^2_{y'}\Psi - 2\frac{\sin\phi}{\cos^2\phi}\partial_{x'y'}\Psi \tag{25}$$

4.1 GL equation in skew coordinates

The Equation 11 in skew coordinates has slightly different form. It has several additional terms compared to cartesian coordinates case. Let us derive its explicit form.

$$\partial_t\Psi = \kappa\vec{D}^2\Psi + \left(1 - |\Psi|^2\right)\Psi \tag{26}$$

where, once again, $\vec{D} = \vec{\nabla} - i\vec{A}$.

All additional terms comes from $\vec{D}^2\Psi$, rest of the equation stays the same

$$\begin{aligned}\vec{D}^2\Psi &= \nabla^2\Psi - i\vec{\nabla}\cdot(\mathbf{A}\Psi) - i\mathbf{A}\cdot\mathbf{D}\Psi - \mathbf{A}^2\Psi \\ &= \sec^2\phi\left(\partial_{x'}^2\Psi + \partial_{y'}^2\Psi - 2\sin\phi\partial_{x'y'}^2\Psi\right) - i\partial_{x'}(A_{x'}\Psi) - i\partial_{y'}(A_{y'}\Psi) \\ &\quad - iA_{x'}\partial_{x'}\Psi - iA_{y'}\partial_{y'}\Psi - (A_{x'}^2 + A_{y'}^2)\Psi - 2\sin\phi A_{x'}A_{y'}\Psi \end{aligned} \tag{27}$$

5 Discretization

Discretization is process of transforming continuous equation into discrete counterpart. It is essential for numerical simulation. Discretization of GL equation has few pitfall which are easy to overlook.

5.1 Link variables

As discussed in subsection 3.1 we have to preserve gauge invariant. In our derivations we relied on scalar potential being zero.

The problem is simple diffrence scheme is not applicable to vector potential, because it do not preserve the gauge. Therefore we have to resort to *link-variables method* that was introduced in [8].

The idea is to use auxiliary variables defined as follows

$$\mathcal{W}^x(x',y') = \exp\left[-i\int_0^{x'} A_{x'}(X,y')dX\right] \tag{28}$$

$$\mathcal{W}^y(x',y') = \exp\left[-i\int_0^{y'} A_{y'}(x',Y)dY\right]. \tag{29}$$

Then express everything in terms of Ψ, $\mathcal{W}^x$ and $\mathcal{W}^y$ and use difference scheme. Using link variables $\vec{D}^2\Psi$ can be written in the following form

$$\begin{aligned}\vec{D}^2\Psi =&\partial^2_{x'}\Psi + \partial^2_{y'}\Psi - i\partial_{x'}(A_{x'}\Psi) - i\partial_{y'}(A_{y'}\Psi) - \\ &- iA_{x'}\partial_{x'}\Psi - iA_{y'}\partial_{y'}\Psi - (A^2_{x'} + A^2_{y'})\Psi + \\ &+ \tan^2\phi\left(\partial_{x'}\Psi^2\partial^2_{y'}\Psi\right) - 2\tan\phi\sec\phi\partial^2_{x'y'}\Psi - 2\sin\phi A_{x'}A_{y'}\Psi \\ =&\overline{\mathcal{W}}^x\partial^2_{x'}\left(\mathcal{W}^x\Psi\right) + \overline{\mathcal{W}}^y\partial^2_{y'}\left(\mathcal{W}^y\Psi\right) + \tan^2\phi\left(\partial^2_{x'}\Psi + \partial^2_{y'}\Psi\right) - \\ &- 2\tan\phi\sec\phi\partial^2_{x'y'}\Psi - 2\sin\phi\left(\overline{\mathcal{W}}^x\partial_{x'}\mathcal{W}^x\right)\left(\overline{\mathcal{W}}^y\partial_{y'}\mathcal{W}^y\right)\Psi\end{aligned} \tag{30}$$

Consequently continuous GL equation becomes

$$\begin{aligned}\partial_t\Psi =&\overline{\mathcal{W}}^x\partial^2_{x'}\left(\mathcal{W}^x\Psi\right) + \overline{\mathcal{W}}^y\partial^2_{y'}\left(\mathcal{W}^y\Psi\right) + \\ &+ \tan^2\phi\left(\partial^2_{x'}\Psi + \partial^2_{y'}\Psi\right) - 2\tan\phi\sec\phi\partial^2_{x'y'}\Psi - \\ &- 2\sin\phi\left(\overline{\mathcal{W}}^x\partial_{x'}\mathcal{W}^x\right)\left(\overline{\mathcal{W}}^y\partial_{y'}\mathcal{W}^y\right)\Psi + \left(1 - |\Psi|^2\right)\Psi\end{aligned} \tag{31}$$

5.2 Semi-implicit method

Another point of discussion is convergence. We cannot use Euler method with skew coordinates, because it will not converge.

We extended the method developed by T. Winiecki and C. S. Adams in order to apply a semi-implicit numerical scheme for integration of the TDGL equations in non-orthogonal coordinates [9]. In this article, the authors show that the semi-implicit method might be more efficient than usual explicit method concerning storage of variables and precision in time. It convergence unconditionally as shown in [10]. As discussed in [9, 11], one can use larger time-steps because of the stability of the method, reducing the computational time of simulations.

5.3 Discrete form

For simplicity, we write the discrete form for each term separately and combine them after.

Let us start with defining *local link variables*

$$W^x_{ij} = \overline{\mathcal{W}}^x_{ij}\mathcal{W}^x_{i+1j} = \exp\left[-i\int_{ih_x}^{(i+1)h_x} A_{x'}(X, y')dX\right] \approx$$
$$\approx \exp\left[-ih_x A_{x'}\left(h_x i + \frac{h_x}{2}, h_y j\right)\right] \tag{32}$$
$$W^y_{ij} = \overline{\mathcal{W}}^y_{ij}\mathcal{W}^y_{ij+1} = \exp\left[-i\int_{jh_y}^{(j+1)h_y} A_{y'}(x', Y)dY\right] \approx$$
$$\approx \exp\left[-ih_y A_{y'}\left(h_x i, h_y j + \frac{h_y}{2}\right)\right] \tag{33}$$

Consider first two terms of Equation 31.

$$\overline{\mathcal{W}}^x_{ij}\partial^2_{x'}\left(\mathcal{W}^x\Psi\right)_{ij} = \overline{\mathcal{W}}^x_{ij}\left(\mathcal{W}^x_{i+1j}\Psi_{i+1j} - 2\mathcal{W}^x_{ij}\Psi_{ij} + \mathcal{W}^x_{i-1j}\Psi_{i-1j}\right) =$$
$$= \left(W^x_{ij}\Psi_{i+1j} - 2\Psi_{ij} + \overline{W}^x_{i-1j}\Psi_{i-1j}\right) = \tilde{\delta}^2_{x'}\Psi_{ij} \tag{34}$$
$$\overline{\mathcal{W}}^y\partial^2_{y'}\left(\mathcal{W}^y\Psi\right)_{ij} = \overline{\mathcal{W}}^y_{ij}\left(\mathcal{W}^y_{ij+1}\Psi_{ij+1} - 2\mathcal{W}^y_{ij}\Psi_{ij} + \mathcal{W}^y_{ij-1}\Psi_{ij-1}\right) =$$
$$= \left(W^y_{ij}\Psi_{ij+1} - 2\Psi_{ij} + \overline{W}^y_{ij-1}\Psi_{ij-1}\right) = \tilde{\delta}^2_{y'}\Psi_{ij} \tag{35}$$

Next two terms are

$$\partial^2_{x'}\Psi_{ij} = \Psi_{i+1,j} - 2\Psi_{ij} + \Psi_{i-1,j} \tag{36}$$
$$\partial^2_{y'}\Psi_{ij} = \Psi_{i,j+1} - 2\Psi_{ij} + \Psi_{i,j-1} \tag{37}$$

The last term becomes

$$\begin{aligned}\left(\overline{\mathcal{W}}^x \partial_{x'}\mathcal{W}^x\right)_{ij}\left(\overline{\mathcal{W}}^y \partial_{y'}\mathcal{W}^y\right)_{ij}\Psi_{ij} = \\ = \frac{1}{h_x h_y}\overline{\mathcal{W}}^x_{ij}\left(\mathcal{W}^x_{ij} - \mathcal{W}^x_{i-1j}\right)\overline{\mathcal{W}}^x_{ij}\left(\mathcal{W}^y_{ij} - \mathcal{W}^y_{ij-1}\right)\Psi_{ij} \\ = \frac{1}{h_x h_y}\left(1 - \overline{W}^x_{i-1j}\right)\left(1 - \overline{W}^y_{ij-1}\right)\Psi_{ij}\end{aligned} \tag{38}$$

Combined together, the equation can be written as

$$\begin{aligned}\Psi^{n+1}_{ij} - \frac{\Delta t}{2}\left(\frac{\tilde{\delta}^2_{x'}}{h^2_x} + \frac{\tilde{\delta}^2_{y'}}{h^2_y}\right)\Psi^{n+1}_{ij} = \Psi^n_{ij} + \frac{\Delta t}{2}\left(\frac{\tilde{\delta}^2_{x'}}{h^2_x} + \frac{\tilde{\delta}^2_{y'}}{h^2_y}\right)\Psi^n_{ij} + \\ + \frac{\Delta t}{2}\left(f^n_{ij} + f^{n+1}_{ij}\right) + \mathcal{O}(\Delta t^2)\end{aligned} \tag{39}$$

where

$$\tilde{\delta}^2_{x'}\Psi_{ij} = W^x_{ij}\Psi_{i+1j} - 2\Psi_{ij} + \overline{W}^x_{i-1j}\Psi_{i-1j} \tag{40}$$
$$\tilde{\delta}^2_{y'}\Psi_{ij} = W^y_{ij}\Psi_{ij+1} - 2\Psi_{ij} + \overline{W}^y_{ij-1}\Psi_{ij-1} \tag{41}$$

And the explicit term in this case becomes:

$$\begin{aligned}f^n_{ij} = \tan^2\phi\left(\frac{\delta^2_{x'}}{h^2_x} + \frac{\delta^2_{y'}}{h^2_y}\right)\Psi^n_{ij} - \frac{1}{4h_x h_y}\frac{\sin\phi}{\cos^2\phi}\delta_x\delta_y\Psi^n_{ij} - \\ - 2\frac{\sin\phi}{h_x h_y}\left(1 - \overline{W}^x_{i-1j}\right)\left(1 - \overline{W}^y_{ij-1}\right)\Psi^n_{ij}\end{aligned} \tag{42}$$

Because the Equation 39 contains $\mathcal{O}(\Delta t^2)$ we can rewrite it as

$$\begin{aligned}\left(\mathbf{1} - r_x\tilde{\delta}^2_x\right)\left(\mathbf{1} - r_y\tilde{\delta}^2_y\right)\Psi^{n+1}_{ij} = \left(\mathbf{1} + r_x\tilde{\delta}^2_x\right)\left(\mathbf{1} + r_y\tilde{\delta}^2_y\right)\Psi^n_{ij} + \\ + \frac{\Delta t}{2}\left(f^{n+1}_{ij} + f^n_{ij}\right) + \mathcal{O}(\Delta t^2)\end{aligned} \tag{43}$$

where $r_x = \Delta t/2h^2_x$ and $r_y = \Delta t/2h^2_y$. This is the form we use in code.

5.4 Vector potential of a constant field

Let us calculate the expression for the link variables. We use the vector potential conveniently as

$$\mathbf{A} = H_e y \mathbf{i} = H_e \cos\phi y' \mathbf{i}' \Rightarrow \mathbf{B} = H_e \mathbf{k}. \tag{44}$$

Then, the link variables become simply:

$$W_{ij}^x = \exp\left(-ih_x H_e \cos\phi h_y j\right), \tag{45}$$

$$W_{ij}^y = \exp(0) = 1. \tag{46}$$

For the sake of better convergence, one should centre y' at the centre of the film.

5.5 Simulation algorithm

Equation 43 binds order parameter at two consecutive time steps. We use it to iteratively update order parameter and find its value at new time steps.

Suppose we know Ψ^n and want to calculate Ψ^{n+1}. Algorithm goes as follows

Step 1: Calculate f^n using Equation 42

Step 2: Calculate Ψ^{n+1} using Equation 43 and approximation $f^{n+1} = f^n$

Step 3: Update explicit term f^{n+1} using newly-found Ψ^{n+1}

Step 4: Update Ψ^{n+1} using updated f^{n+1} found in step 3

Step 5: Repeat steps 3 and 4 three times

In simulations we do up to 5000 time increases.

6 Results

We ran simulations for parallelogram-shaped superconducting thin film. We consider the case where the film is surrounded by a hard ferromagnetic material, *i.e.* a material that does not allow formation of Cooper pairs and reduces the order parameter to zero at the boundary of the superconductor. Also, this material is considered to be in its demagnetized state, *i.e.* its total magnetization is zero and it is not affected by the applied field.

We varied angle ϕ, external magnetic field and applied current. The external magnetic field is perpendicular to the film and spatially constant (but vary with time in some simulations). Sketch of modeled shape is shown in Figure 1.

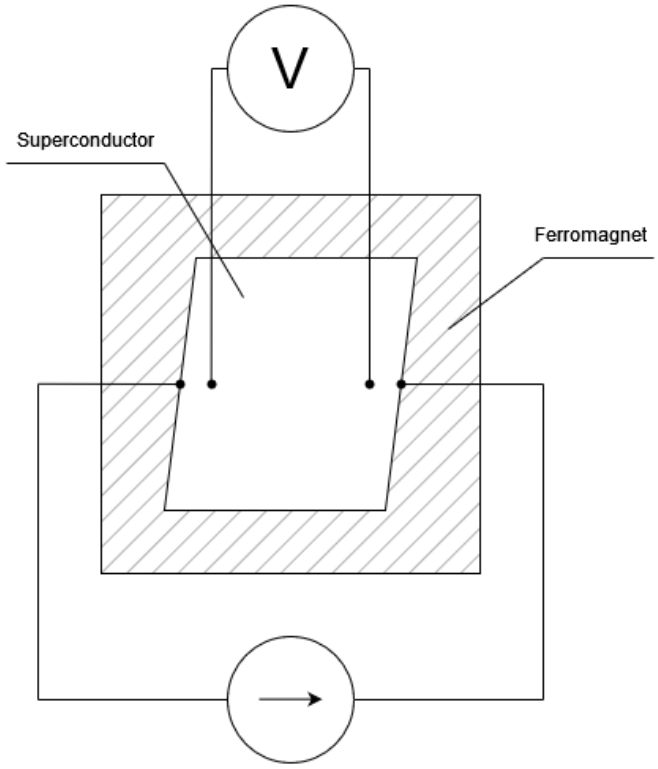

Figure 1: Sketch of shape used in simulations

In the following results the parameters used were: $\Delta t = 0.01$, $h_x = h_y = 0.5$ (mesh cell size) and $N_x = N_y = 64$ (mesh size).

6.1 Zero magnetic field and zero current

At zero magnetic field, the solution should converge to a stationary case where the order parameter starts at $|\Psi|^2 = 0$ (normal state) at the boundary and increases

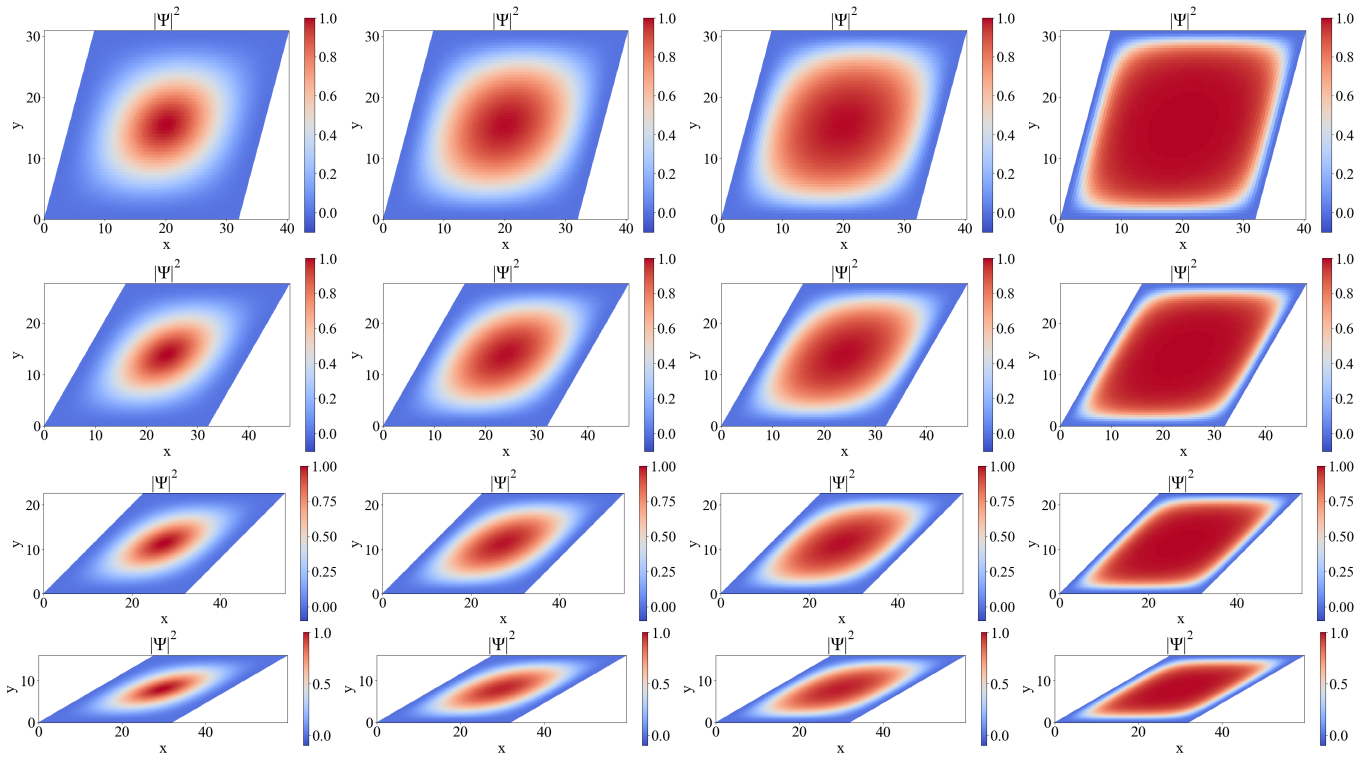

Figure 2: Plots of $|\Psi|^2$, for angles (first row) $\phi = \pi/12$, a), b), c), d), (second row) $\phi = \pi/6$, d), e), f), g), (third row) $\phi = \pi/4$, h), i), j), k), (fourth row) $\phi = \pi/3$, l), m), n), o). The snapshots in each row are taken at times $t = 0,\ 0.05,\ 0.01\ 0.25$, respectively.

to $|\Psi|^2 = 1$ (full superconducting state) at a distance approximately equal to the coherence length ξ.

For example, consider the situation where the initial condition is bell-shaped — order parameter is one in center and smoothly decays to zero on boundary.

$$\Psi(x', y', t = 0) = \sin\left(\frac{\pi}{N_x h_x} x'\right) \sin\left(\frac{\pi}{N_y h_y} y'\right). \tag{47}$$

Results for this initial condition are shown in Figure 2. Ψ relaxes as expected, going to stable state where inner points are superconducting, boundary is not and change from one to other is rather sharp (because ξ is small).

Another initial condition to exemplify the robustness of the numerical method is the so-called *quenched* state. It simulates the case when the material is brought abruptly from the normal to the superconducting state, where the order parameter is just a random variable without phase coherence.

$$\Psi(x', y', t = 0) = \frac{\zeta_r}{\sqrt{2}} + i\frac{\zeta_i}{\sqrt{2}}, \tag{48}$$

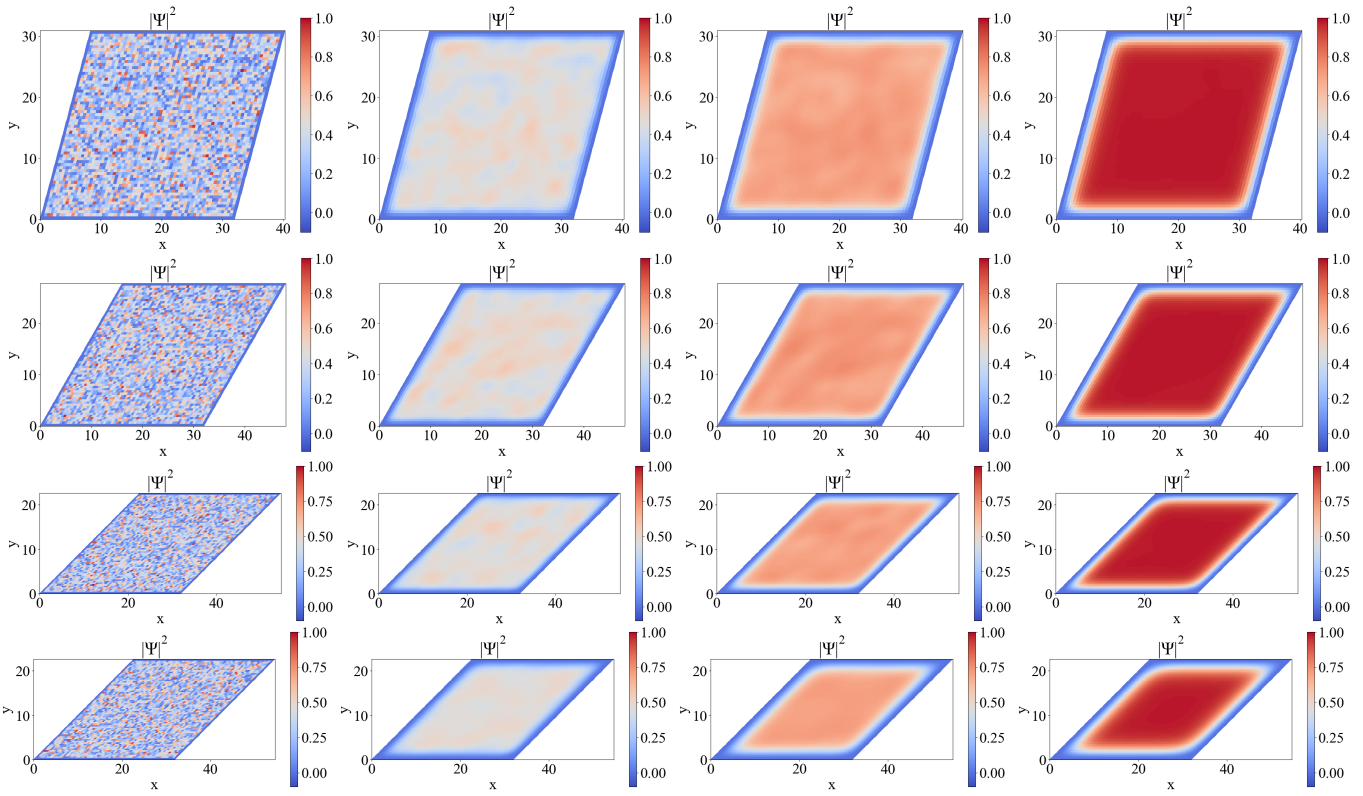

Figure 3: Plots of $|\Psi|^2$, for angles (first row) $\phi = \pi/12$, a), b), c), d), (second row) $\phi = \pi/6$, d), e), f), g), (third row) $\phi = \pi/4$, h), i), j), k), (fourth row) $\phi = \pi/3$, l), m), n), o). The snapshots in each row are taken at times $t = 0,\ 0.05,\ 0.01\ 0.25$, respectively.

where ζ_r and ζ_i are random numbers between 0 and 1 numbers sorted for each mesh point.

Figure 3 shows quenched state. Simulation results once again agree with intuition and experiments — no matter what initial state is, the superconductor relaxes to the same stable state when no magnetic field is present.

Another observation can be made: normal state area is bigger around sharp corners (compare images in last column of Figure 3). It is known fact that magnetic field penetrates superconductor from edges first (see [12], [13] for discussion on GL in wedge), but appears in simulations as well.

The maximum of the order parameter stays rather unchanged for moderate angles, but it significantly reduces its value for angles extremely close to $\pi/2$. In this case, the order parameter cannot recover from zero to one in such small space between the edge and the center of the film. This can be seen in Figure 4

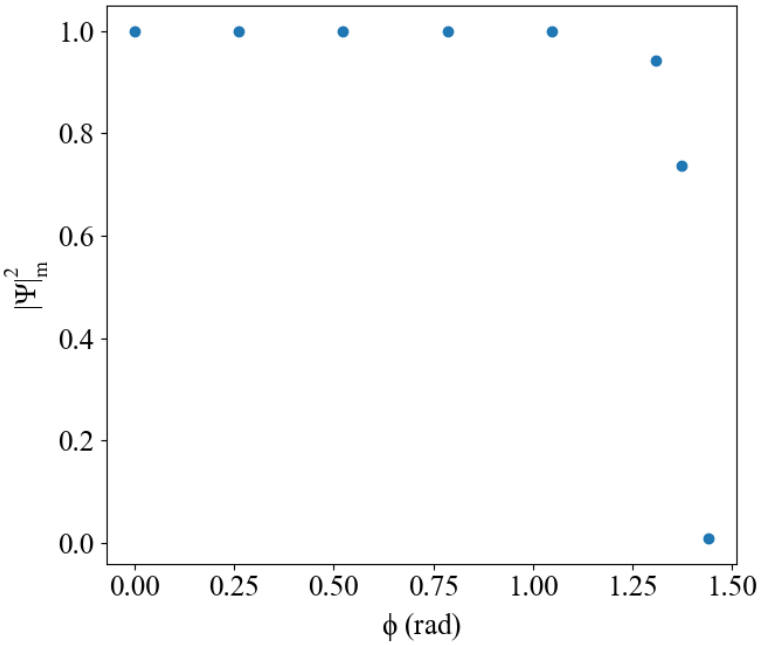

Figure 4: Maximum value of the modulus of the order parameter along the film, $|\Psi|^2_m$, for parallelograms with the same side but different angles, ϕ.

6.2 With applied magnetic field

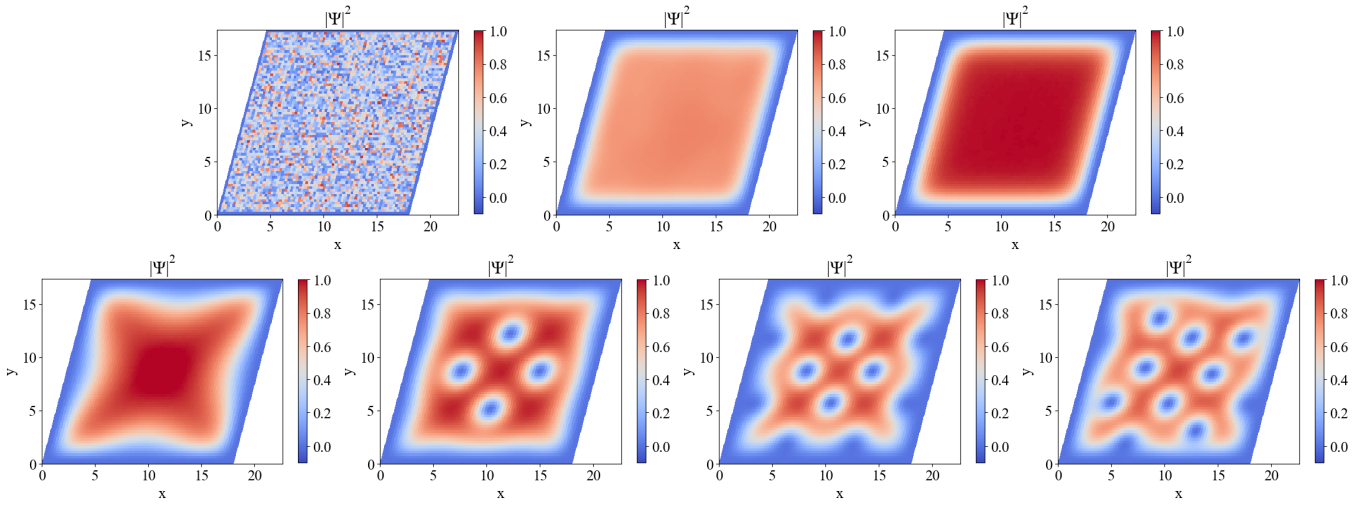

Figure 5: Plots of $|\Psi|^2$, for $\phi = \pi/12$. The snapshots in each row are taken at times $t = 0,\ 1,\ 2$ at the first row and $t = 200,\ 300,\ 400,\ 500$ at the second row.

If strong enough external magnetic field is present, *vortices* (normal-state dots with quantized flux) appear. In this set of simulations we gradually increase magnetic field strength as time passes. Figure 5 ($\phi = \pi/12$) and Figure 6 ($\phi = \pi/3$) show state of the film at different points in time (and consequently at different external magnetic field).

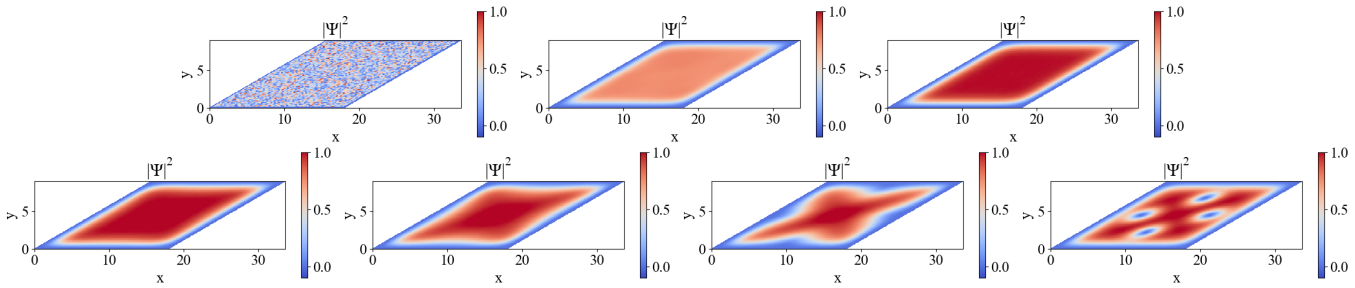

Figure 6: Plots of $|\Psi|^2$, for $\phi = \pi/3$. The snapshots in each row are taken at times $t = 0,\ 1,\ 2$ at the first row and $t = 200,\ 300,\ 400,\ 500$ at the second row.

For vortex to appear flux of magnetic field through the film must be greater than *magnetic flux quantum* $\Phi_0 = h/2e$. Therefore weak magnetic field can not form vortices. The flux of magnetic field directly depends on area of the film, which in turn depends on $\cos\phi$. The greater ϕ, the lower area of the film and flux, therefore critical field is stronger. We can see it from simulation as well — at $t = 20$ (second left figure in bottom row) vortices already formed in Figure 5 and only starting to appear in Figure 6.

Another interesting effect can be seen at stronger fields (for example, last image of Figure 5. Vortices repel each other, because two small vortices are more energy-efficient than big vortex combining two. It leads to asymmetry and fluctuations. It appears there may be some circulating motion. We did not study it, but it can be a topic of future research.

6.3 Systems with applied magnetic field and moderate current

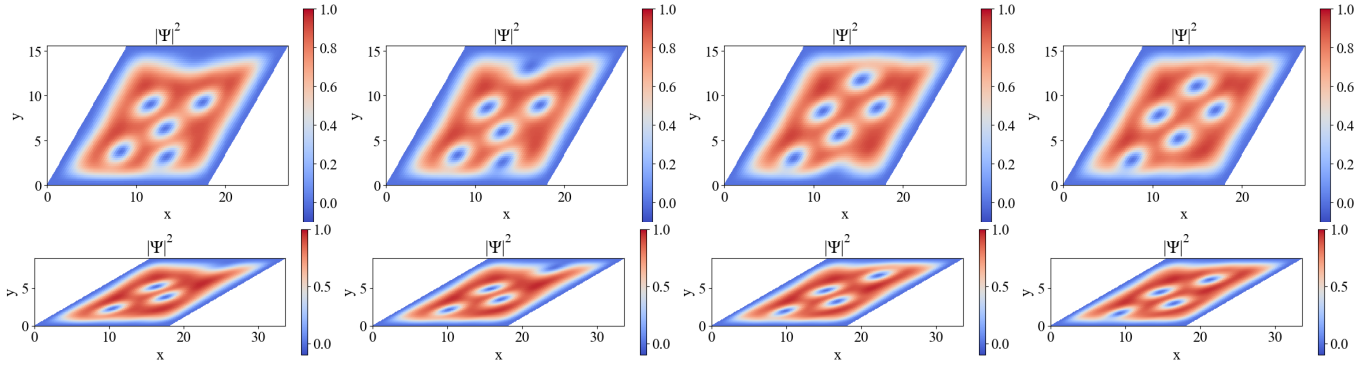

Figure 7: Plots of $|\Psi|^2$, for angles (first row) $\phi = \pi/6$, (second row) $\phi = \pi/3$. The snapshots in each row are taken at times $t = 23,\ 25,\ 27,\ 29$, respectively.

Similar to previous increasing magnetic field case, but we add constant current that flows from east boundary to west. As result we observe drift of vortices in perpendicular

direction (from north to south). As we can see in Figure 7 vortices are born at the north boundary, slowly move and disappear at the south boundary.

For comparsion images in Figure 7 are taken at the same timestamps. It is clear, that vortices move faster in the first row. We are not ready to provide explanation for this phenomenon.

6.4 System with higher current

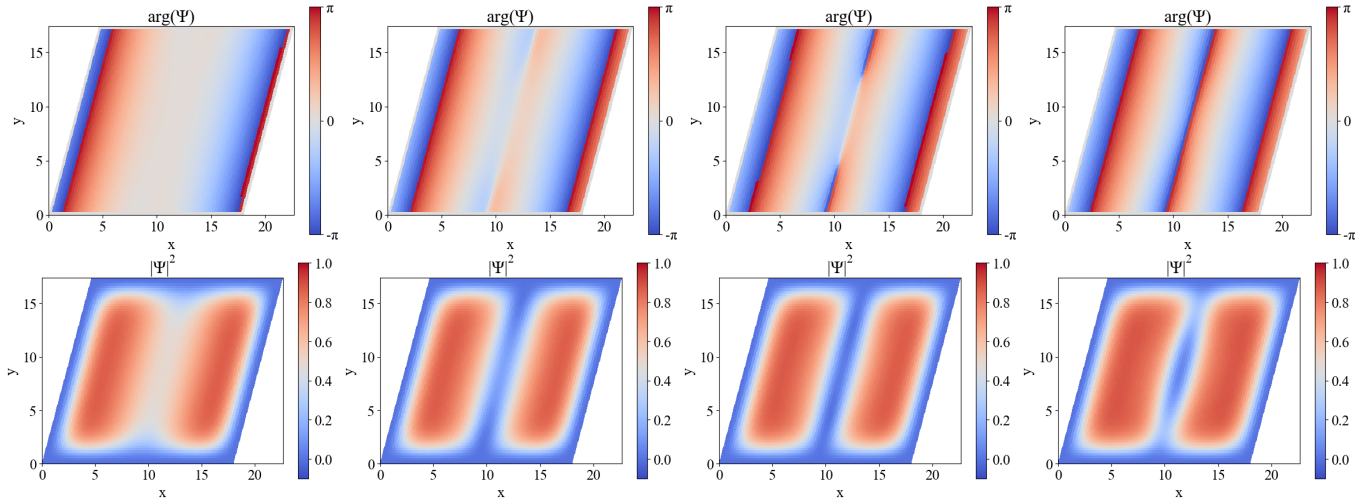

Figure 8: Plots of phase of Ψ (first row), $|\Psi|^2$ (second row). The snapshots in each row are taken at times $t = 6.8,\ 7.8,\ 8,\ 8.2$, respectively.

Last set of simulations consider case with applied current and zero magnetic field. It is rather interesting and unique case. Let's say we have current flow from east boundary to west one. It induces magnetic field around it. Said magnetic field penetrate north boundary of the film and similarly to subsection 6.3 creates "imaginary" vortex. Same happens around south boundary, but magnetic field and vortex have opposite direction. Then those two vortices start moving, but because they face opposite directions they move in opposite directions as well. North vortex drift south and south vortex drift north. This happens because vortices with opposite magnetic field direction should feel opposite forces from the current, a phenomenon related to the popular "Magnus effect" [14, 15]. In the middle they meet and annihilate, and the process starts over. This phenomenon was reported in similar systems [16]. It can be seen on plots of the order parameter in Figure 8. Note that the vortex/anti-vortex pair is situated at the center of the film. Pay close attention to middle of each image.

In the upper row of Figure 8, one can see the plots for the phase of the order parameter and in the lower row, the modulus. The time sequence happens from left to

right. During the dynamic event, a pair vorter/anti-vortex starts penetrating by the center of the sample and, although there is no singularity of the phase yet, a severe reduction of the modulus is seen on the second frame. Then, strictly speaking, the vortices are inside the film only at the third column. At the last time frame on the right, it is shown the recovery of the modulus of the order parameter. Also, the phase has a discontinuity line but not singular points, *i.e.* the pair annihilated itself.

Therefore if we were to measure resistance between contact points we would see oscillating pattern of it going up and down.

6.5 Discussion

In the previous case, where it was applied current to the film, vortex/anti-vortex pair appeared in the center of the film and annihilated themselves. The resistance of the film should become higher if measured from one side to the other as sketched in Figure 1. This should happen because the superconducting condensate cannot percolate throughout the system. It is interesting to note that this is a feature periodic in time found in the current-voltage (I-V) characteristics of films [16]. Although we did not show these peaks in resistivity quantitatively, we can make a qualitative inference of this phenomenon by noting that there are clearly two isolated superconducting regions in Figure 7. For extremely high currents, the order parameter drops down to zero, which means that the material becomes a usual conductor where Ohm's law applies. Therefore, the overall picture of the IV characteristics of thin films if confirmed as in [17].

7 Conclusion

The method developed in this thesis generalized the standard method for describing mesoscopic thin films for cases with non-orthogonal coordinates. By mesoscopic, we mean that the system is large enough in comparison with atomic distances but still it is small enough so that the boundaries are relevant to determine its characteristics. It is known that the vortex lattice in mesoscopic superconductors is strongly dependent on the shape of the boundaries [18]. In our results, we decided to use a sample with the shape of a parallelogram and we verified that, indeed, stationary and dynamic states are strongly influenced by the angle in the corners. In the case of a zero-field and zero-current simulation, we verified that the method is robust with respect to the initial conditions. Indeed, we confirmed that the system relaxes to the same stationary solution for two different initial states (quenched and localized). For extreme values of the angle in the side of the parallelogram, we verified that superconductivity disappears. In the case of applied magnetic field, the number of vortices becomes smaller with the angle. This is reasonable since the total area of the film becomes smaller with larger inclinations. In the case of applying both field and currents, we obtained the flux flow phase with number of vortices simultaneously in the film also dependent of the angle. Finally, we considered the case of larger applied current and zero external field. In this case, pairs of vortex/anti-vortex appeared and annihilated each other periodically along a central line also inclined with respect to the vertical, *i.e.* it followed the shape of the boundaries. We expect that the results in this thesis might inspire the production of metamaterials with superconducting films with the shape we use or even more complex.

8 References

[1] H.K. Onnes. "The Superconductivity of Mercury". In: *Comm. Phys. Lab. Univ.* (1911).

[2] J. Bardeen, L. N. Cooper, and J. R. Schrieffer. "Microscopic Theory of Superconductivity". In: *Phys. Rev.* 106 (1 Apr. 1957), pp. 162–164. DOI: 10.1103/PhysRev.106.162. URL: https://link.aps.org/doi/10.1103/PhysRev.106.162.

[3] Jia-Yuan Dai and Phillipo Lappicy. "Ginzburg–Landau Patterns in Circular and Spherical Geometries: Vortices, Spirals, and Attractors". In: *SIAM Journal on Applied Dynamical Systems* 20.4 (Jan. 2021), pp. 1959–1984. ISSN: 1536-0040. DOI: 10.1137/20m1378739. URL: http://dx.doi.org/10.1137/20M1378739.

[4] Jose Barba Ortega, Jesus Gonzalez, and Miryam Rincón Joya. "Numerical solution of the time-dependent Ginzburg-Landau equation for a superconducting mesoscopic disk: Link variable method". In: *Journal of Physics Conference Series* 410 (Feb. 2013), pp. 2008–. DOI: 10.1088/1742-6596/410/1/012008.

[5] L. D. Landau. "On the theory of phase transitions". In: *Zh. Eksp. Teor. Fiz.* 7 (1937). Ed. by D. ter Haar, pp. 19–32. DOI: 10.1016/B978-0-08-010586-4.50034-1.

[6] V.L. Ginzburg and L.D. Landau. "On the theory of superconductivity". In: *Zh. Eksp. Teor. Fiz.* 20 (1950), pp. 1064–1082.

[7] J. Pearl. "Current Distribution in Superconducting Films Carrying Quantized Fluxoids". In: *Applied Physics Letters* 5 (Aug. 1964), pp. 65–66. DOI: 10.1063/1.1754056.

[8] Kenneth G. Wilson. "Confinement of quarks". In: *Phys. Rev. D* 10 (8 Oct. 1974), pp. 2445–2459. DOI: 10.1103/PhysRevD.10.2445. URL: https://link.aps.org/doi/10.1103/PhysRevD.10.2445.

[9] T. Winiecki and C.S. Adams. "A Fast Semi-Implicit Finite-Difference Method for the TDGL Equations". In: *Journal of Computational Physics* 179.1 (2002), pp. 127–139. ISSN: 0021-9991. DOI: https://doi.org/10.1006/jcph.2002.7047. URL: https://www.sciencedirect.com/science/article/pii/S0021999102970476.

[10] J W Thomas. *Numerical partial differential equations: Finite difference methods*. en. 1st ed. Texts in Applied Mathematics. New York, NY: Springer, Nov. 1998.

[11] M. Holt and N.N. Yanenko. *The Method of Fractional Steps: The Solution of Problems of Mathematical Physics in Several Variables*. Springer Berlin Heidelberg, 2012. ISBN: 9783642651083. URL: https://books.google.ru/books?id=q6LwCAAAQBAJ.

[12] S.N. Klimin et al. "Superconductivity in a wedge with a small angle: an analytical treatment". In: *Solid State Communications* 111.10 (1999), pp. 589–594. ISSN: 0038-1098. DOI: https://doi.org/10.1016/S0038-1098(99)00226-4. URL: https://www.sciencedirect.com/science/article/pii/S0038109899002264.

[13] F. Brosens et al. "Superconductivity in a wedge: analytical variational results". In: *Solid State Communications* 111.10 (1999), pp. 565–569. ISSN: 0038-1098. DOI: https://doi.org/10.1016/S0038-1098(99)00227-6. URL: https://www.sciencedirect.com/science/article/pii/S0038109899002276.

[14] N. B. Kopnin and V. E. Kravtsov. "Forces acting on vortices moving in a pure type II superconductor". In: *Zh. Eksp. Teor. Fiz.* 71.4 (1976).

[15] E. B. Sonin. "Magnus force in superfluids and superconductors". In: *Phys. Rev. B* 55 (1 Jan. 1997), pp. 485–501. DOI: 10.1103/PhysRevB.55.485. URL: https://link.aps.org/doi/10.1103/PhysRevB.55.485.

[16] G. R. Berdiyorov, M. V. Milo ševi ć, and F. M. Peeters. "Kinematic vortex-antivortex lines in strongly driven superconducting stripes". In: *Phys. Rev. B* 79 (18 May 2009), p. 184506. DOI: 10.1103/PhysRevB.79.184506. URL: https://link.aps.org/doi/10.1103/PhysRevB.79.184506.

[17] B. I. Ivlev and N. B. Kopnin. In: *Usp. Fiz. Nauk* 142.435 (1984).

[18] Rafael Zadorosny et al. "Crossover between macroscopic and mesoscopic regimes of vortex interactions in type-II superconductors". In: *Phys. Rev. B* 85 (21 June 2012), p. 214511. DOI: 10.1103/PhysRevB.85.214511. URL: https://link.aps.org/doi/10.1103/PhysRevB.85.214511.